Cold Regions Science and Technology 74–75 (2012) 21–30

Contents lists available at SciVerse ScienceDirect

Cold Regions Science and Technology

journal homepage: www.elsevier.com/locate/coldregions

Topographic curvature effects in applied avalanche modeling

Jan-Thomas Fischer [a,*], Julia Kowalski [b], Shiva P. Pudasaini [c]

[a] Federal Research and Training Centre for Forests, Natural Hazards and Landscape, BFW, Department of Natural Hazards and Alpine Timberline, Rennweg 1, A-6020 Innsbruck, Austria
[b] WSL Institute for Snow and Avalanche Research SLF, Flüelastr. 11, CH-7260 Davos Dorf, Switzerland
[c] Department of Geodynamics and Geophysics, Steinmann Institute, University of Bonn, Nußallee 8, 53115 Bonn, Germany

ARTICLE INFO

Article history:
Received 16 May 2011
Accepted 7 January 2012

Keywords:
Snow
Avalanche
Dynamics
Modeling
Natural terrain
Curvature
Centrifugal force
Friction coefficients

ABSTRACT

This paper describes the implementation of topographic curvature effects within the RApid Mass MovementS (RAMMS) snow avalanche simulation toolbox. RAMMS is based on a model similar to shallow water equations with a Coulomb friction relation and the velocity dependent Voellmy drag. It is used for snow avalanche risk assessment in Switzerland. The snow avalanche simulation relies on back calculation of observed avalanches. The calibration of the friction parameters depends on characteristics of the avalanche track. The topographic curvature terms are not yet included in the above mentioned classical model. Here, we fundamentally improve this model by mathematically and physically including the topographic curvature effects. By decomposing the velocity dependent friction into a topography dependent term that accounts for a curvature enhancement in the Coulomb friction, and a topography independent contribution similar to the classical Voellmy drag, we construct a general curvature dependent frictional resistance, and thus propose new extended model equations. With three site-specific examples, we compare the apparent frictional resistance of the new approach, which includes topographic curvature effects, to the classical one. Our simulation results demonstrate substantial effects of the curvature on the flow dynamics e.g., the dynamic pressure distribution along the slope. The comparison of resistance coefficients between the two models demonstrates that the physically based extension presents an improvement to the classical approach. Furthermore a practical example highlights its influence on the pressure outline in the run out zone of the avalanche. Snow avalanche dynamics modeling natural terrain curvature centrifugal force friction coefficients.

1. Introduction

In the last century, hazard mapping gained a high importance in land-use planning of alpine regions (Barbolini et al., 2000; Gruber and Margreth, 2001; Pudasaini and Hutter, 2007). In this process, areas of increased hazard risk are defined which is either prohibited or subject to additional protective requirements to create new infrastructure or civil engineering works. For already existing constructions, the potential of additional mitigation measures is investigated. Both, a realistic risk assessment and the design of protective measures require experience and a high level of expert knowledge. In order to gain further insight into avalanche flow heights, flow velocities, run-out distances and impact pressures avalanche simulation models became a more and more important tool for decision makers and practitioners. Avalanche simulations are especially helpful when analyzing large scale scenarios or when one is interested in the response to a change in the input data. Gruber and Bartelt (2007), for instance, proposed an automated way of defining release area and release heights and performed a large scale analysis in order to identify the forest as a protective measure.

Two of the most important existing mathematical avalanche theories are the Saint Venant model for shallow water flow and the Savage-Hutter-type models for shallow granular flows. Savage and Hutter (1989) derived a system of one dimensional depth-averaged equations for shallow granular flow. Several important generalizations to this model have been derived to higher dimensions and complex topographies (Gray et al., 1999) and incorporate non-trivial topography, model the flows in curved and twisted channels and over realistic terrains (Pudasaini and Hutter, 2003, 2007; Pudasaini et al., 2005a,b). Because of its influence on the apparent driving force and the normal and the lateral pressures (as demonstrated in Denlinger and Iverson, 2004; Iverson et al., 2004; McDougall and Hungr, 2004; Patra et al., 2005; Pitman et al., 2003a,b; Pudasaini et al., 2005b, 2008; Wieland et al., 1999), the surface curvature of the avalanche path is of particular interest.

The theory for shallow granular or debris flows are rigorously derived and confirmed by experiments or data (Denlinger and Iverson, 2004; Gray et al., 1999; Iverson et al., 2004; McDougall and Hungr, 2004; Patra et al., 2005; Pitman et al., 2003a,b; Pudasaini and Hutter, 2003, 2007; Pudasaini and Kroener, 2008; Pudasaini et al., 2005a,b, 2008; Wieland et al., 1999). The dynamics of an avalanche

* Corresponding author at: Federal Research and Training Centre for Forests, Natural Hazards and Landscape, BFW, Department of Natural Hazards and Alpine Timberline, Rennweg 1, A-6020 Innsbruck, Austria. Tel.: +43 512 573933 5102.
E-mail address: jt.fischer@uibk.ac.at (J.-T. Fischer).

0165-232X/$ – see front matter © 2012 Elsevier B.V. All rights reserved.
doi:10.1016/j.coldregions.2012.01.005

is governed by driving forces due to gravitational acceleration and resisting forces due to friction and also the lateral pressure gradients. Savage-Hutter-type equations are based on the Mohr–Coulomb closure for the Cauchy stress (Savage and Hutter, 1989). The basal friction relations reduce to curvature corrected dry Coulomb terms, (see, e.g., Gray et al., 1999; Hutter et al., 2005; Pudasaini and Hutter, 2003, 2007; Wieland et al., 1999). When required, the Coulomb friction can be complemented by a velocity dependent drag term (Pudasaini, 2011; Pudasaini and Hutter, 2007). However, it still remains a challenge to directly implement these models for generic mountain topographies into an existing numerical simulation model.

For practical purposes, heuristically motivated Saint Venant type avalanche models are in use which incorporate an empirical friction relation. In the avalanche simulation software RAMMS (RApid Mass MovementS), on which our work is based upon, the friction law is given by a dry Coulomb term superposed by a velocity dependent drag. In the avalanche community, this model is commonly referred to as the Voellmy–Salm model (Bartelt et al., 1999; Salm, 1993). RAMMS computes avalanche velocity and flow heights over realistic terrain given by digital elevation models (DEM) (Christen et al., 2010). The model calibration is based on back calculation of observed avalanches and depends implicitly on avalanche track characteristics such as the curvature of the avalanche track (Gruber and Bartelt, 2007; Salm et al., 1990).

A tendency in the past years has clearly been the development of two separate branches of avalanche dynamics research. The first focuses on the derivation from first principles and analysis of consistent, comprehensive, depth-averaged, granular flow models (Gray et al., 1999; Pudasaini and Hutter, 2003, 2007; Pudasaini et al., 2005a, b; Savage and Hutter, 1989). The other branch is based on relatively simple mathematical models that can easily be implemented for complex terrain and that rely on calibration of the model parameters and are not constrained physically, neglecting some of the underlying physical and geometric processes (Bartelt et al., 1999; Gruber and Bartelt, 2007; Salm, 1993).

Our work is a step forward to theoretically include curvature effects into the practical implementation of the avalanche simulation toolbox, RAMMS. We will briefly recall on different modeling approaches to include curvature and introduce a local curvature correction into the existing model. We decompose the velocity dependent friction into a topography dependent term that accounts for a curvature correction in the dry Coulomb friction, and a topography independent contribution similar to the classical Voellmy friction term. With this decomposition and construction of the general curvature dependent friction, we propose a new 'extended Voellmy–Salm model' and implement it into RAMMS. Finally, with three site-specific examples, we compare the apparent frictional resistance with the extended Voellmy–Salm model against the classical Voellmy–Salm frictional resistance without topographic curvature. Our results demonstrate substantial effects of the curvature in the avalanche dynamics and thus highlight the importance of curvature effects in applied avalanche modeling.

2. Mathematical models for avalanches

Depth-averaged avalanche models in general constitute a system of hyperbolic conservation laws. They have the structure of the shallow water equations (Gray et al., 1999; Pudasaini and Hutter, 2003, 2007; Pudasaini et al., 2005a,b; Savage and Hutter, 1989). The avalanche model equations describe the time evolution of the flow height h and the surface tangent flow velocity components $\mathbf{u}=(u_x, u_y)^T$. These state variables are summarized in the state vector $\mathbf{V}=(h, hu_x, hu_y)^T$. These are functions of space $\mathbf{x}=(x,y)$ and time t. Here, the subscripts x and y indicate that the surface tangential flow velocity components are derived along the direction of the horizontal coordinate axes x and y in a fixed Cartesian coordinate system. The coordinate system is chosen such that the z-axis is parallel to the direction of the gravitational acceleration ($\mathbf{g}_0=(0,0,-g)^T$, g is the gravity constant). The vector form of the model is

$$\partial_t \mathbf{V}(\mathbf{x},t) + \nabla\cdot\mathbf{F}(\mathbf{V}(\mathbf{x},t)) = \mathbf{S}(\mathbf{V}(\mathbf{x},t)), \tag{1}$$

in which $\nabla=(\partial_x,\partial_y)^T$ denotes the partial derivative with respect to space, $\mathbf{F}(\mathbf{V})$ represents the transport fluxes and $\mathbf{S}(\mathbf{V})$ represents the source terms (net driving forces) with

$$\mathbf{F}(\mathbf{V}) = \begin{pmatrix} hu_x & hu_y \\ hu_x^2 + g_z\frac{h^2}{2} & hu_xu_y \\ hu_xu_y & hu_y^2 + g_z\frac{h^2}{2} \end{pmatrix}; \mathbf{S}(\mathbf{V}) = \begin{pmatrix} 0 \\ S_x \\ S_y \end{pmatrix}. \tag{2}$$

In $\mathbf{F}(\mathbf{V})$, the first components are associated with the mass conservation, and the second and the third components related to the momentum conservation; along the x and y directions, respectively. Entrainment and deposition processes are neglected. The momentum transport fluxes also include the convective fluxes ($hu_x^2, hu_y^2; hu_xu_y$) and the hydrostatic pressure contribution ($g_zh^2/2$). Here, $\mathbf{g}=(g_x,g_y,g_z)^T$ represents the components of the gravitational acceleration in the surface induced down-slope, cross-slope and normal directions, respectively, as functions of the horizontal Cartesian coordinates (see Fig. 1 and Section 3 for a more detailed description). The source terms $\mathbf{S}$ include the components of the net driving forces (including driving gravity and resisting friction terms). In applied avalanche simulations these friction relations are empirically motivated and often the main focus of a calibration work (Gruber and Bartelt, 2007; Sailer et al., 2008; Salm et al., 1990; Sampl and Zwinger, 2004). In the following section the concept of the Voellmy friction relation is presented in detail. Note that in Eq. (2) for simplicity the pressure is assumed to be isotropic. Isotropic models are applied to study shock waves and oblique shocks in granular flows down inclined planes with or without obstacles (Cui et al., 2007; Gray and Cui, 2007; Gray et al., 2003; Hákonardóttir and Hogg, 2005). However, for a discussion on anisotropic pressure distribution in granular flows, we refer to Pudasaini and Hutter (2007) and Pudasaini and Kroener (2008).

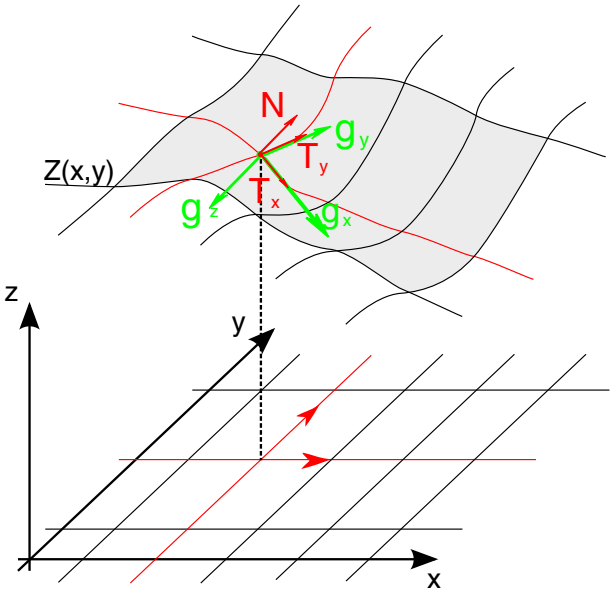

Fig. 1. The topography ($\mathfrak{S}_{DEM}(x,y)$) of an surface given in a Cartesian coordinate system x,y,z. z points in the direction of the gravitational acceleration. The surface induces the vector triad $\{\mathbf{T_x},\mathbf{T_y},\mathbf{N}\}$ and the local components of the gravitational acceleration system $\mathbf{g}=(g_x,g_y,g_z)^T$ in the direction of the surface induced $\{\mathbf{T_x},\mathbf{T_y},\mathbf{N}\}$.

2.1. Classical Voellmy friction relation

The Voellmy friction relation (Voellmy, 1955) has been applied to avalanche simulations since the mid 1960s. In the context of the shallow water models, it became the basis of the dynamic simulation for snow avalanches in RAMMS. The dynamics of the flow are predominately influenced by the net forces in x and y directions denoted by $S_i, i \in \{x,y\}$ (compare with Eq. (1)). They are given by a superposition of gravitational acceleration and frictional resistance:

$$S_i = \underbrace{hg_i}_{\text{gravitational force}} \underbrace{-\frac{u_i}{\|\mathbf{u}\|}\left(h\mu g_z + \frac{g}{\xi}\mathbf{u}^2\right)}_{\text{frictional forces}}. \quad (3)$$

$$\textit{friction parameters}: \mu, \xi.$$

The two empirical friction parameters μ and ξ represent the dry Coulomb friction and velocity dependent viscous drag (friction), respectively. In the original Voellmy–Salm approach, μ is independent of material properties but varies with the mountain profile. However experiments on the laboratory scale (Platzer et al., 2007; Pudasaini and Hutter, 2007; Pudasaini and Kroener, 2008; Pudasaini et al., 2005a,b) and on the large field scale (Bartelt et al., 2006; Sovilla et al., 2008) indicate, that this assumption is not true in general. The velocity dependent friction is characterized by the parameter ξ and was first stated by (Voellmy, 1955) as 'turbulent' friction. It is important to note that later, (Salm, 1993) stated that ξ should mainly depend on the terrain geometry and interpreted it as 'viscous' friction. Furthermore, as an extension of the frictional model (Bartelt et al., 2006) and (Buser and Bartelt, 2009) couple the Coulomb friction coefficient μ and the Voellmy drag ξ to an additional field variable for random kinetic energy of the fluctuating motion in an avalanche. In a recent work, Bartelt et al. (2007) proposed a friction law in which the friction coefficient μ varies between two limits μ_1 and μ_2 from the front to the tail of an avalanche as an inverse exponential transition function of the gravitational work rate.

A different approach modeling the basal frictional resistance was pioneered by Pouliquen (1999a,b) by modifying the dry Coulomb friction, proposing a new empirical scaling law for the flow of granular material down rough incline. In this law the friction coefficient μ is expressed in terms of the mean velocity and the thickness of the granular layer. This includes two angles: θ_1, an angle where $h_{stop}(\theta)$ diverges, and θ_2, an angle where $h_{stop}(\theta)$ vanishes, where $h_{stop}(\theta)$ is the minimum thickness necessary to observe steady uniform flow at inclination θ. This model includes two further parameters β: a fit parameter, and L a characteristic dimensionless thickness over which $h_{stop}(\theta)$ varies. The expression for $h_{stop}(\theta)$ is derived from $\mu(u,h) = \tan\theta_1 + (\tan\theta_2 - \tan\theta_1)\exp\left(-\frac{\beta h}{Ld}\frac{\sqrt{gh}}{u}\right)$ and $\frac{u}{\sqrt{gh}} = \beta\frac{h}{h_{stop}(\theta)}$, where d is the particle diameter. Thus, θ_1, θ_2 and L are characteristics of material. This friction law has successfully been extended and applied to granular flows (Johnson and Gray, 2011; Mangeney et al., 2007; Pouliquen and Forterre, 2002). However, these authors mainly focus their attention on the hydrostatic pressure, rough and mild slopes close to or below the internal friction angle where the flow takes place on a layer of glued particles of the same size and shape. These flows are close to jamming, intermittent, slow, uniform, and steady, and could thus adjust their velocities. In contrast, we are dealing with different flow conditions where the flow takes place on steep and relatively smooth slope thus inducing rapid motion. Furthermore, we do not need the explicit knowledge of the critical slope of the free surface in the dynamic simulation of rapid flows. This is automatically taken into account by the pressure gradient. For more detail on this we refer to Pudasaini and Kroener (2008) and Pudasaini (2011).

The real origin of the contribution of ξ to the basal topography and thus to the overall friction law is still open for discussion. However, modeling results with RAMMS have been promising. Although μ and ξ still lack a proper physical explanation, 60 years of acquired avalanche data in the Swiss Alps made a systematic calibration possible. Today, practical avalanche simulations rely on a rigorous project to calibrate the friction parameters μ and ξ (Gruber and Bartelt, 2007). According to the Swiss Guidelines (SG) (Salm et al., 1990), values for μ and ξ can be prescribed manually, or alternatively for large scale simulations, automated procedure (based on GIS that classifies the terrain) determines the friction coefficients. This process is based on a DEM analysis to distinguish between different terrain features such as open slope, channel, gully, forest or non-forest regions. Additionally, parameters including altitude above sea level, return period and avalanche size lead to the final μ and ξ classification. Fig. 2 shows the classification of ξ for three different natural avalanche paths according to the Swiss Guidelines.

2.2. Models including curvature effects

Savage and Hutter (1989) developed a continuum mechanical model for rapid granular flows which has also been used to model avalanche flows (Pudasaini and Hutter, 2007). A Mohr–Coulomb friction relation is assumed. Various extensions to this theory appropriately account for a complex bottom topography. Gray et al. (1999) proposed a two-dimensional depth-integrated theory for gravity driven free surface flow over a moderately curved surface in the downslope direction. A further generalization is attributed to Pudasaini and Hutter (2003), which introduces the effects of curvature as well as twist of channels into the avalanche models. The advantage of this model is that it theoretically and systematically decomposes the gravity load into three non-zero components in the down-slope, cross-slope and the surface normal direction, respectively. To our knowledge, Pudasaini and Hutter (2003) and Pudasaini et al. (2005a,b) models are the only models in avalanche and debris flow dynamics which have the property of systematically including non-zero gravity acceleration components as driving forces in the respective curvilinear coordinate directions following the channel. This model has been applied in modeling the granular and debris avalanches down curved and twisted channels with channel following coordinates (see Pudasaini and Hutter, 2003, 2007; Pudasaini et al., 2005a,b; Pudasaini et al., 2008). In their approach a predefined master curve is adjusted to a flow channel. In a next step a curvilinear coordinate system is constructed originating from the master curve. The transformation into the space-curve based coordinate system gives insight into the effects of non-uniform curvature and torsion of the avalanche path in the avalanche dynamics.

In the process of transforming the model equations into a curvilinear coordinate system, additional terms arise in the frictional force. The normal force (overburden pressure) gains an extra term, which accounts for a 'centrifugal force' (Pudasaini and Hutter, 2003, 2007; Pudasaini et al., 2005a,b) associated with the curvature. Again, this contribution to the basal friction depends on the underlying topography and the flow velocity. This contribution can be directly calculated from the DEM and a calibration step is not necessary.

In addition to the above mentioned granular flow theories, Bouchut et al. (2003) and Bouchut and Westdickenberg (2004) also provide alternative shallow granular flow models. Although the derivation of different mass flow theories differ fundamentally from one another, the general mathematical form of the model equations is the same as in Eq. (1) and the source terms can be compared.

2.3. A curvature dependent Voellmy friction relation

2.3.1. A new approach

The goal of this work is to mathematically and physically accurately include the curvature effects into the Voellmy–Salm model by using the coordinate parameterization in the RAMMS computational tool. To achieve this, the curvature effects described by the sophisticated

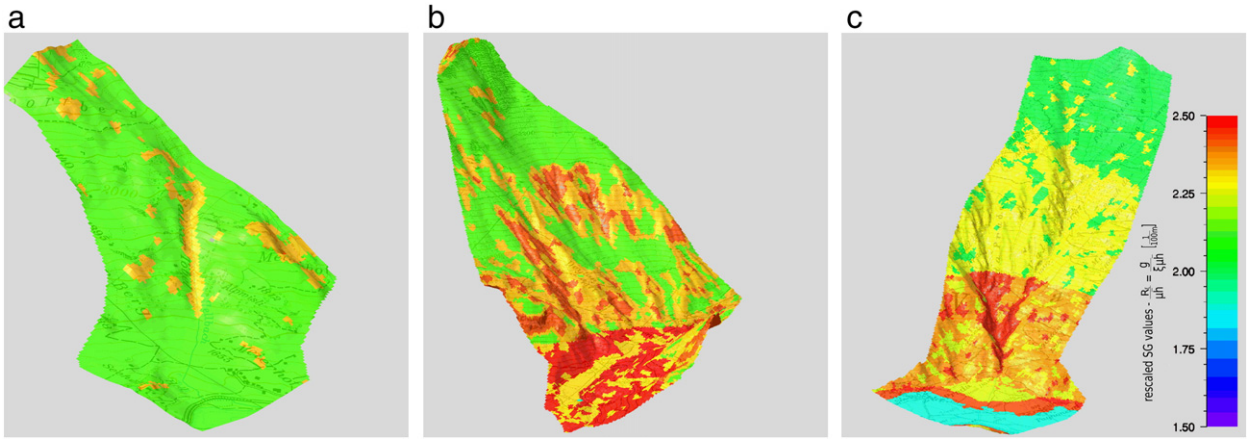

Fig. 2. Three Swiss mountain terrains (DTM-AV ©2008 swisstopo (DV033492), map PK25 ©2008 swisstopo (DV033492)) prone to snow avalanches: Salezertobel (a), Vallee de la Sionne (b), and Val Prada (c); showing calibrated Swiss Guideline (SG) friction parameter. In order to make the absolute values comparable to the mean curvature (Fig. 3) a rescaled form according to $\frac{g}{\mu h \xi} = \frac{R_\xi}{\mu h}$, $\bar{h} = 1m$ is displayed here. Calibration maps are according to the automatic terrain classification.

mathematical models for granular flows (Pudasaini and Hutter, 2003) are adopted to the classical Voellmy–Salm friction relation. A non orthogonal local coordinate system (see, Christen et al., 2010; Pudasaini et al., 2003) is adopted which can be applied directly on the given DEM data. In our approach, the extra term (curvature contribution) in the frictional resistance arises from the projection of additional acceleration in the surface normal direction. This extra curvature-dependent frictional resistance will ultimately be associated with the Coulomb friction term.

In contrast to the classical Voellmy–Salm friction relation in which both friction parameters are empirical values, that are accessible only through calibration work, we split the velocity dependent friction contribution into two parts. To compare the basal curvature-induced additional friction term with the classical velocity dependent friction, we define the dimensionless resistance parameters R_t and R_ξ. The static part, denoted by $R_\xi = g/\xi$ represents the velocity dependent friction in the Voellmy–Salm (VS) model. It accounts for the empirical velocity dependent friction (viscous drag) and in contrast to the SG calibration it is assumed to be independent of the mountain profile and represents the influence of the snow properties. In analogy to the theories including curvature effects (Pudasaini and Hutter, 2007), a second terrain dependent contribution R_t originates from the basal surface curvature $\mathbf{K}$, and is an additional contribution to the normal force as an extra 'centrifugal' term. This extra centrifugal force effect will then be transferred to the basal shear stress through the frictional Coulomb sliding law.

We choose a formulation of the net driving forces which includes the classical VS friction coefficient R_ξ and the curvature dependent new friction coefficient R_t. This formulation allows a direct comparison of the two friction parameters (R_t and R_ξ). Finally, the terrain dependent friction effects are associated with the Coulomb frictions terms. We re-write the components of the net driving forces (S_i, $i \in \{x,y\}$) as:

$$S_i = hg_i - \frac{u_i}{\|\mathbf{u}\|}\left(h\mu g_z + R_t\mathbf{u}^2 + R_\xi\mathbf{u}^2\right), \qquad R_t = \mu h\frac{\mathbf{u}^T\mathbf{K}\mathbf{u}}{\mathbf{u}^2},\ R_\xi = \frac{g}{\xi}. \tag{4}$$

Eq. (4) implemented in Eq. (2) will be referred to as the 'extended Voellmy–Salm model'. The resistance parameter R_t contains all the spatial variations of the field variables (height and velocities) and the mountain topography, whereas R_ξ is static. Note that if the mountain curvature vanishes then $R_t = 0$. In this case (4) reduces to Eq. (3) and that the extended and classical model are identical. In Section 4, we formally derive R_t, which is new to the classical Voellmy–Salm model.

3. Modeling mountain topography

The mountain topography is constructed through a DEM with spatial resolutions between 2 and 25 m. In order to accurately account for the basal topography we formulate a moving vector triad based on the surface DEM ($\Im_{DEM}$) given by a sufficiently smooth profile function $Z(x,y)$, in the Cartesian horizontal-vertical form:

$$\Im_{DEM}(x,y) = \begin{pmatrix} x \\ y \\ Z(x,y) \end{pmatrix}. \tag{5}$$

We define the surface induced tangent vectors $\mathbf{T}_x(x,y)$ and $\mathbf{T}_y(x,y)$ on $\Im_{DEM}$, such that their projections onto the xy plane are parallel to the associated x and y axis. $\mathbf{N}(x,y)$ is the outer normal to the surface. Following the usual procedure in practice (Christen et al., 2010) the vector triad are defined as follows:

$$\mathbf{T}_x := \frac{1}{\sqrt{1+\partial_x Z^2}}\begin{pmatrix} 1 \\ 0 \\ \partial_x Z \end{pmatrix}, \tag{6}$$

$$\mathbf{T}_y := \frac{1}{\sqrt{1+\partial_y Z^2}}\begin{pmatrix} 0 \\ 1 \\ \partial_y Z \end{pmatrix}, \tag{7}$$

$$\mathbf{N} := \frac{1}{\sqrt{1+\partial_x Z^2+\partial_y Z^2}}\begin{pmatrix} \partial_x Z \\ \partial_y Z \\ -1 \end{pmatrix}. \tag{8}$$

With this, the local components of the gravitational acceleration can be expressed in terms of the surface induced directions $\{\mathbf{T}_x, \mathbf{T}_y, \mathbf{N}\}$:

$$g_x = \mathbf{T}_x \cdot \mathbf{g}_0,\ g_y = \mathbf{T}_y \cdot \mathbf{g}_0,\ g_z = \mathbf{N} \cdot \mathbf{g}_0, \tag{9}$$

where $\mathbf{g}_0 = (0,0,-g)^T$, '$\cdot$' denotes the dot product, and g_x, g_y, g_z are the projections of $\mathbf{g}_0$ along the directions of $\mathbf{T}_x, \mathbf{T}_y, \mathbf{N}$, respectively.

An arbitrary surface $\Im_{DEM}$ can be parameterized in many different ways depending on the choice of the coordinate system. Fig. 1 shows a reference surface $\Im_{DEM}(x,y)$ in a Cartesian coordinates $\{x,y,z\}$. The surface induced vector triad $\{\mathbf{T_x}, \mathbf{T_y}, \mathbf{N}\}$ generates the local components of the gravitational acceleration $(g_x, g_y, g_z)^T$. As in Pudasaini and Hutter (2003), $\{\mathbf{T_x}, \mathbf{T_y}, \mathbf{N}\}$ are non-orthogonal, so are the components of $(g_x, g_y, g_z)^T$.

4. Equation of motion on arbitrary surface

It is important to note that, the model equations used in RAMMS are solved in a fixed Cartesian coordinate system whereas the models including curvature are formulated in 'quasi-curvilinear coordinate systems' along the mountain topography. As already described in the previous sections this transformation into a curvilinear coordinate system naturally leads to a modification of the surface normal gravity component and thus modification of the normal load which leads to the modification of the Coulomb friction terms in the final model equations. In our new approach, the implementation and calculation method has been developed such that it includes curvature and can still be employed in the existing model structure of RAMMS. In this section we describe the derivation of the equations of motion for a masspoint attached to a surface in Cartesian coordinates. In order to do so we use the well known Lagrange formulation of classical mechanics.

The Lagrange equation $L=T-V$ (here, T: kinetic energy, V: potential energy) in Cartesion coordinates (with coordinates $q_i=\{x,y,z\}$ and their time derivative $\frac{d}{dt}q_i(t)=\dot{q}_i(t)$) for a free moving masspoint in the gravitational potential field is:

$$L(q_i(t),\dot{q}_i(t))=\frac{m}{2}\left(\dot{x}(t)^2+\dot{y}(t)^2+\dot{z}(t)^2\right)-mgz(t), \tag{10}$$

with the constraint of moving along a fixed surface given by a sufficiently smooth profile function $Z(x,y)$:

$$z(t)=Z(x(t),y(t)). \tag{11}$$

Solving the Euler–Lagrange Equations $\frac{d}{dt}\frac{\partial L}{\partial \dot{q}}-\frac{\partial L}{\partial q}=0$ and including the constraint (11) we obtain the equations of motion:

$$\begin{pmatrix}\ddot{x}\\ \ddot{y}\\ \ddot{z}\end{pmatrix}=\begin{pmatrix}-\dfrac{\partial_x Z\left(g+\dot{x}(t)^2\partial_x^2 Z+2\dot{x}(t)\dot{y}(t)\partial_x\partial_y Z+\dot{y}(t)^2\partial_y\partial_y Z\right)}{1+\partial_x Z^2+\partial_y Z^2}\\ -\dfrac{\partial_y Z\left(g+\dot{x}(t)^2\partial_x^2 Z+2\dot{x}(t)\dot{y}(t)\partial_x\partial_y Z+\dot{y}(t)^2\partial_y^2 Z\right)}{1+\partial_x Z^2+\partial_y Z^2}\\ \dfrac{-g\left(\partial_x Z^2+\partial_y Z^2\right)+\dot{x}(t)^2\partial_x^2 Z+2\dot{x}(t)\dot{y}(t)\partial_x\partial_y Z+\dot{y}(t)^2\partial_y^2 Z}{1+\partial_x Z^2+\partial_y Z^2}\end{pmatrix}. \tag{12}$$

We observe that due to the constraint of moving on a trajectory embedded in the surface, we obtain extra velocity dependent terms in the acceleration. In addition to the acceleration due to the projections of the gravitational acceleration in titx and y directions, we obtain velocity (i.e., $\dot{x}(t),\dot{y}(t)$) dependent terms including derivatives in x and y direction accounting for variations of the surface function $Z(x(t),y(t))$. These terms are associated with a 'centrifugal force'.

4.1. Mathematical description of a curvature tensor

The description of curvature that is applicable to the existing model structure of RAMMS is a combination of the mathematical description of the topography (see Section 3) and the equations of motion of a mass moving on a fixed surface (as explained above). The constraint of moving along the fixed surface $\Xi_{DEM}=(x,y,Z(x,y))^T$ induces additional acceleration components (Eq. (12)). The projection of this additional acceleration in normal direction, (Eq. (8)) leads to an extra 'centripetal' term in the normal force. It can be written in terms of the surface function $Z(x,y)$ and its spatial gradients:

$$\begin{pmatrix}\ddot{x}\\ \ddot{y}\\ \ddot{z}\end{pmatrix}\cdot\mathbf{N}=\frac{\dot{x}(t)^2\partial_x^2 Z+2\dot{x}(t)\dot{y}(t)\partial_x\partial_y Z+\dot{y}(t)^2\partial_y^2 Z}{\sqrt{1+\partial_x Z^2+\partial_y Z^2}}. \tag{13}$$

This velocity dependent acceleration in normal direction to the basal surface includes terms accounting for the surface variation and its curvature.

Note that the velocity components in the Lagrangian framework $(\dot{x}(t),\dot{y}(t))$ are the projections along the Cartesian axis. Whereas the velocities in the VS model $\mathbf{u}=(u_x,u_y)^T$ are the surface parallel velocities. This yields the relation:

$$\begin{pmatrix}\dot{x}(t)\\ \dot{y}(t)\end{pmatrix}=\begin{pmatrix}\dfrac{1}{\sqrt{1+\partial_x Z^2}}u_x\\ \dfrac{1}{\sqrt{1+\partial_y Z^2}}u_y\end{pmatrix}. \tag{14}$$

With the unit vectors $\mathbf{e}_i$ in the direction of the Cartesian axis ($i=x,y,z$):

$$cos\,\zeta_i=\frac{1}{\sqrt{1+\partial_i Z^2}}=\mathbf{T}_i\cdot\mathbf{e}_i,\quad i=x,y, \tag{15}$$

where, ζ_i denotes the angle of surface inclination in $i=x$ and $i=y$ direction, respectively.

Motivated by the expression (13), we can explicitly formulate the surface curvature in terms of the surface function and its spatial derivatives with the following definitions:

$$\begin{aligned}K_X&:=\frac{\partial_x^2 Z}{(1+\partial_x Z^2)\sqrt{1+\partial_x Z^2+\partial_y Z^2}},\\ K_{XY}&:=\frac{\partial_x\partial_y Z}{\sqrt{1+\partial_y Z^2}\sqrt{1+\partial_x Z^2}\sqrt{1+\partial_x Z^2+\partial_y Z^2}},\\ K_Y&:=\frac{\partial_y^2 Z}{\left(1+\partial_y Z^2\right)\sqrt{1+\partial_x Z^2+\partial_y Z^2}}.\end{aligned} \tag{16}$$

This can be written in tensor form:

$$\mathbf{K}:=\begin{pmatrix}K_X & K_{XY}\\ K_{XY} & K_Y\end{pmatrix}. \tag{17}$$

Now from Eqs. (13), (14), (16), and (17) the additional curvature and velocity dependent normal component of the acceleration can be written as

$$\frac{R_t\mathbf{u}^2}{\mu h}=u_x^2K_X+2u_xu_yK_{XY}+u_y^2K_Y=\mathbf{u}^T\mathbf{K}\mathbf{u}. \tag{18}$$

It is important to note the following. If $K_{XY}=0$, then $R_t\mathbf{u}^2=\mu h(u_x^2K_X+u_y^2K_Y)$. If the slope is flat in the lateral direction, then $K_Y=0$ and that $R_tu_x^2=\mu hu_x^2K_X$, which is the curvature term in Savage and Hutter (1991) and Gray et al. (1999) models and Pudasaini and Hutter (2003) model without the twist (i.e., $\eta=1$). The formulations (16) and (18) allow the determination of the curvature tensor and thus the new resistance function R_t for each point of the given mountain topography in a preprocessing step. The algorithm to compute the additional component of the normal acceleration can then be implemented in the program code of the existing RAMMS model. Fig. 3 displays the result of the mean of the curvature components K_X and K_Y, (i.e., $K_{mean}=\frac{K_X+K_Y}{2}$) for three different natural avalanche paths in the Swiss Alps. Naturally more channelized terrain regions appear to generate high curvatures. The automatic friction parameter classification of the Swiss Guidelines (Fig. 2) shows a high correspondence with the mean of the curvature components (Fig. 3). This appears naturally due to the calibration dependence on different terrain features which are related to terrain curvature.

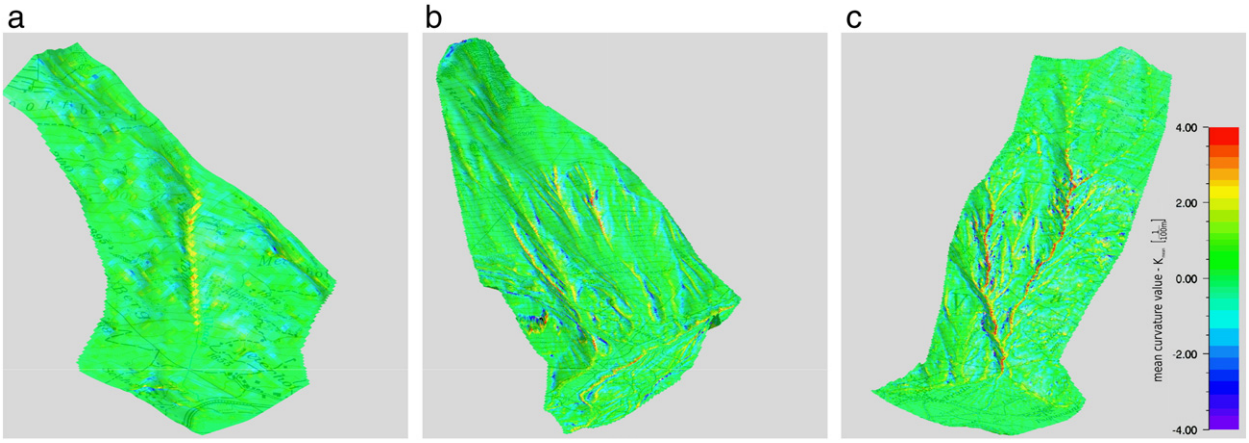

Fig. 3. Map and DEM (DTM-AV ©2008 swisstopo (DV033492), map PK25 ©2008 swisstopo (DV033492)) of the three mountain terrains prone to snow avalanches: Salezertobel (a), Vallee de la Sionne (b) and Val Prada (c); Showing mean of the curvature components $\kappa_{mean} = \frac{K_X + K_Y}{2}$, high mean curvature values (red) indicate gullies/channels, low (negative) mean curvature values (blue) indicate ridges.

5. Simulation examples

5.1. RAMMS

RApid Mass MovementS (RAMMS) is a computer simulation model designed by the SLF (Institute for Snow and Avalanche Research) as a practical tool for avalanche practitioners. The model Eqs. (1) and (2) are solved with a first and second-order accurate HLLE-Heun numerical scheme (Christen et al., 2010). RAMMS has been calibrated and tested for a series of well-documented avalanches of the Swiss avalanche database. Therefore, the model results can be used to estimate run-out distances, flow velocities, flow heights and impact forces. A graphical visualization of the numerical calculations is provided to evaluate the simulation results. Geo-referenced maps or aerial photographs can also be imported into RAMMS and then superimposed on the computational domain which makes the interpretation of model results easier.

To perform numerical calculation RAMMS needs three basic input quantities.

- *Release zone area and fracture height.* This information provides the knowledge about the avalanche volume and therefore has a strong influence on the avalanche dynamics.
- *The DEM.* All information about the complexity and geometry of the natural terrain are provided by the DEM. The spatial DEM resolution has a dominant impact on the flow dynamics and avalanche path.
- *Model friction parameters.* Classically, the model incorporates two friction parameters, μ and ξ which represent dry coulomb and velocity dependent viscous friction, respectively.

In the following simulation examples the friction relation implemented in RAMMS has been enhanced with the extended model (4) with Eq. (18).

5.2. Avalanche flows in natural terrain

To interpret and outline the importance of the curvature dependent extended Voellmy–Salm friction (drag) relation (Eq. (4) with Eq. (18)), numerical calculations are performed on three avalanche paths using the RAMMS toolbox. The curvature effects are highly dependent on the underlying topography and the actual avalanche path. The performance of the extended model along three different natural avalanche flow paths in Switzerland is presented here (Fig. 4). The Salezertobel avalanche path (left) is located close to the SLF Research Institute in Davos, Canton Graubuenden; the Val Prada avalanche path (right) is located on the south side of the Alps in the Canton Graubuenden. The Vallee de la Sionne avalanche path (center) is a SLF test site for real scale avalanches and located in the Canton Valais. The given DEM resolution is 10 m × 10 m. The flow of the Salezertobel is mostly aligned with the topographic features whereas the Val Prada avalanche path is highly curved and twisted. The flow on the Vallee de la Sionne experiences a slight run up on the opposite valley side as observed in the field. In all three simulations, underlying topography guides the flow.

Large avalanches of a 300-year return period are simulated for all three mountain slopes according to the Swiss guidelines. The corresponding initial data for an avalanche of this kind are an approximate volume of $>60{,}000\ m^3$, this corresponds to a snow mass of $>18{,}000$ ton (300 kg m^{-3} snow density). For the three avalanche paths this corresponds to the release areas of $30{,}000 - 60{,}000\ m^2$ with surface normal release heights ranging from 1 to 2 m. Fig. 4 displays the snow avalanche flow heights in three different avalanche paths at two time steps ($t_1 = 40$ s, $t_2 = 100$ s, the top and bottom panels, respectively) after release. Important in these simulations is that we systematically and explicitly included the mountain curvature in the avalanche dynamics through R_t, which could not be included in RAMMS with the classical Voellmy–Salm model, because for classical Voellmy–Salm model $R_t = 0$.

One of the main aims of this paper is to compare the spatially dependent friction parameters according to the classification calibration method described in Section 2.1 with our new approach. As a further reference we consider the general constant friction parameters ($\bar{\mu} = 0.2$, $\bar{\xi} = 2000$). In practice, these spatially constant parameters are used for a rough estimations or in regions without a specified calibration. In order to assign the results we define the following three approaches with different friction parameter settings:

- VS_{SG}: Classical VS approach with varying friction parameters ($\mu = \mu_{SG}$ and $R_\xi = g/\xi_{SG}$ according to the Swiss Guidelines, $R_t = 0$), compare Fig. 2.
- VS_{const}: Classical VS approach with constant friction parameters ($\mu = \bar{\mu}$, $R_\xi = g/\bar{\xi}$, $R_t = 0$).
- $VS_{extended}$: Extended VS approach with constant friction parameters ($\mu = \bar{\mu}$, $R_\xi = g/\bar{\xi}$) and the terrain curvature dependent resistance $R_t = \mu h \frac{\mathbf{u}^T \mathbf{K} \mathbf{u}}{\mathbf{u}^2}$, compare Fig. 3.

We analyze the influence of the friction parameters on simulation results for three avalanche paths. Changing the friction coefficients implies a change in all model results, such as the evolution of flow height or flow velocity. Further, this influences the most important model results (for practical application), the run out. In this section we are not aiming for a comparison of the model results but the dimensionless resistance values R_t, R_ξ and $R_t + R_\xi$ themselves. This is done for each of the three different approaches mentioned above with respect to the three simulation examples.

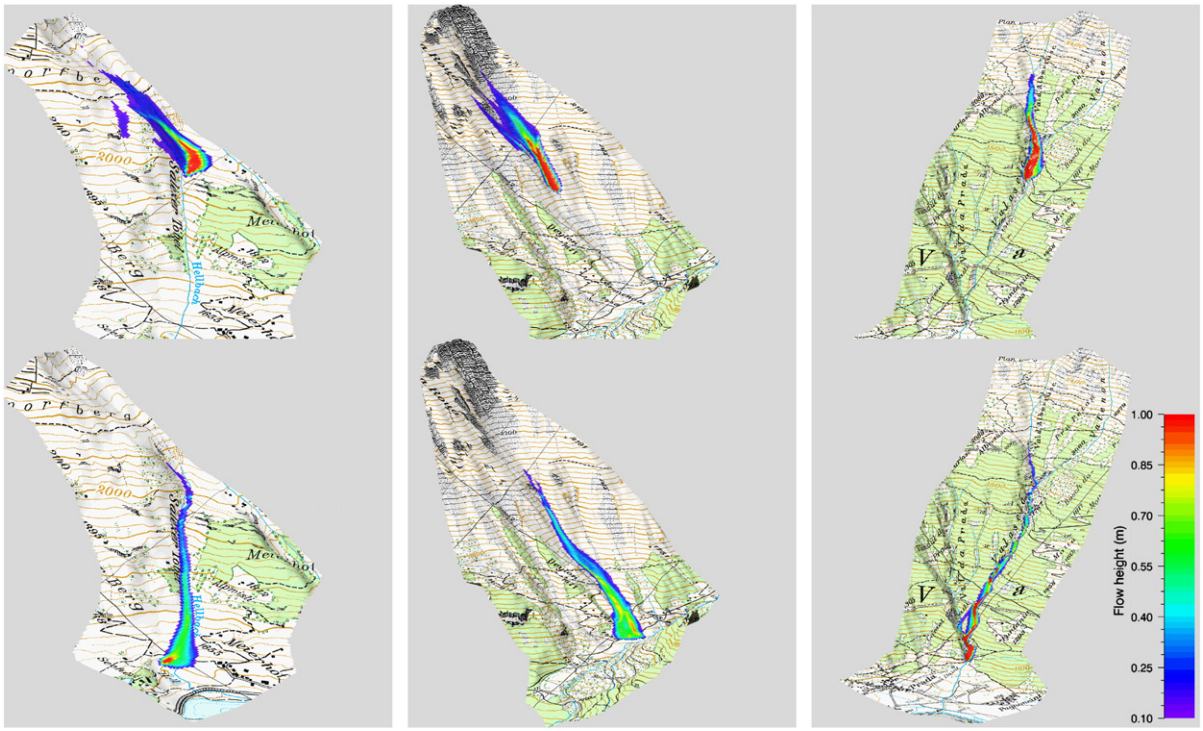

Fig. 4. Three avalanche simulation examples (DTM-AV ©2008 swisstopo (DV033492), map PK25 ©2008 swisstopo (DV033492)) in the Swiss Alps with the extended Voellmy–Salm model with $R_\xi = g/\bar{\xi}$ (according to the SG) showing flow height for two specific time steps ($t_1 = 40$ s, $t_2 = 100$ s, the upper and lower panels, respectively), from release to run out: Salezertobel, Davos, canton Graubuenden (left); Vallee de la Sionne, canton Valais (center); and Val Prada, Canton Graubuenden (right). The flow is guided by the underlying topography.

On the one hand, the resistance values $R_\xi = g/\xi_{SG}$ according to the VS_{SG} approach are automatically calibrated and are constant in time but vary in space. Similarly, by definition the resistance values according to the VS_{const} are constant in time and constant in space. On the other hand, the systematically calculated R_t friction value of the $VS_{extended}$ approach vary in time and space, due to its dependency on the flow velocity, flow height and the topographic curvature. In order to compare the spatially corresponding resistance values R_t, R_ξ and $R_t + R_\xi$ we consider the maximum values R_t over time. Furthermore, the values of the VS_{SG} approach are a discrete spatial distribution of about 5 classes of possible friction values (compare with Fig. 2), while the maximum of the curvature dependent resistance values R_t of $VS_{extended}$ is continuous in space (compare with the mean of the curvature components $\kappa_{mean} = \frac{K_X + K_Y}{2}$, Fig. 3). In order to obtain a result that can be interpreted quantitatively, we plot the linear interpolation of the resistance values of the different approaches. With this, the general trend of the difference in the three approaches can be analyzed. Fig. 5 presents a quantitative comparison of the resistance values as obtained from the simulation results with the different approaches. For this comparison, the classical Swiss Guidelines (VS_{SG}) and the general constant parameter (VS_{const}) approach serve as a standard references. Naturally, the resistance parameters according to VS_{SG} approach superpose for the three different avalanche paths. This is due to the fact that the parameter calibration classifications are the same for each example. Same holds for the VS_{const} approach with the constraint that there is only one constant parameter class.

All results are plotted against the resistance values ($R_\xi = g/\xi_{SG}$) of the VS_{SG} approach. Naturally the resistance values ($R_\xi = g/\xi_{SG}$) of the VS_{SG} (red line) appear as the bisectrix. On the other extreme, the resistance values ($R_\xi = g/\bar{\xi}$) of VS_{const} are represented by a constant (black line) and show much less correlation with resistance values ($R_t + R_\xi$) of the $VS_{extended}$ approach. In our avalanche simulation examples, we observed considerable differences in the magnitude of R_t for three flow paths. This is so, because for extended Voellmy Salm model R_ξ is associated with constant friction parameters. Then, the changes in $R_t + R_\xi$ for different flow paths are the direct measures of changes in R_t associated with the topographic curvatures of corresponding mountain slopes. In the Salezertobel (cyan line) the avalanche motion is mainly in a longitudinal channel direction. So, $R_t + R_\xi$ deviates substantially from $R_\xi = g/\xi_{SG}$. The typical release zone in the Valee de la Sionne (green line) induces a flow direction slightly oblique to the relevant topography. An additional curvature effect is due to the run up on the opposite valley side. The Val Prada (blue line) avalanche path is highly twisted and thus the flow experiences significant curvature effects. The same tendency is observed

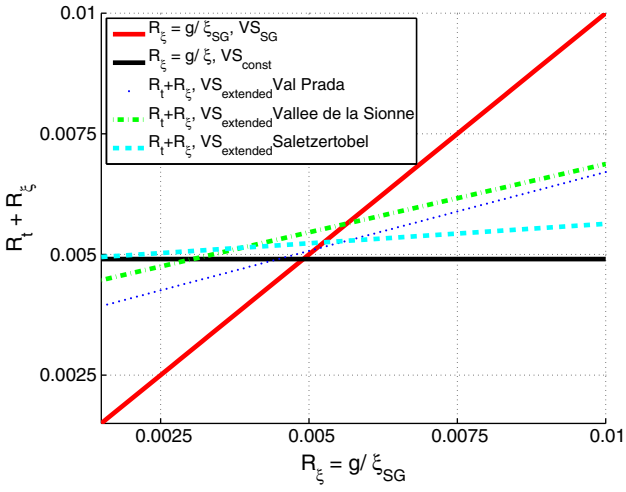

Fig. 5. Shown are the dimensionless resistance values corresponding to the different avalanche paths and resistance approaches plotted against the resistance values ($R_\xi = g/\xi_{SG}$) of the VS_{SG} approach. The resistance values are: $R_\xi = g/\xi_{SG}$ according to the VS_{SG} and $R_\xi = g/\bar{\xi}$ according to the VS_{const} approach; and $R_t + R_\xi$ according to the $VS_{extended}$ approach that includes the terrain curvature.

when comparing the maximum height and velocity values directly. So, the interesting result is that, the correlation between the extended VS model and the classical VS model (using the Swiss Guidelines) highly depends on the chosen avalanche path. In particular, we see that it is not the shape of the flow channel itself, but rather the degree of alignment of the main flow direction and the channel that determines the correlation between these two models. In general, we see a significant correlation between the resistance values of the $VS_{extended}$ approach and the classical VS_{SG} approach using the Swiss Guidelines as long as curvature terms are considered that are aligned with the flow direction. However, it is important to note that the classical VS model with the Swiss Guidelines, the friction parameters are calibrated values without any direct physical basis, whereas in the extended VS model, μ and R_ξ are spatially constant values, but the topographic curvature dependent friction parameter R_t is entirely new, physically based and includes the actual flow dynamics. With physical–mathematical arguments, we have systematically constructed the curvature of the mountain slope, R_t. The other parameters μ and R_ξ can be modeled or constrained differently, examples include the variable friction parameters as explained with the random kinetic energy of the fluctuating motion (Bartelt and Buser, 2010). This way, all the topography curvature and the friction parameters are (or can be) constrained in the avalanche simulation.

5.3. Practical importance of the new model

Here, we demonstrate the practical importance of our new extended model with an example. From a physical point of view, the dynamics and magnitude of the spatial variation of the friction coefficient R_t are of main interest as this can demonstrate the contrast between the different model approaches. For a practitioner or a decision maker, perhaps the most important dynamic quantity is the outline of the peak pressure expected by the avalanche (mainly in the run-out zone). Maximum impact pressures ($\rho\mathbf{u}^2$, where $\rho = 300\ \mathrm{kg\ m^{-3}}$ is the snow bulk density) are obtained by taking the calculated maximum values over time throughout the avalanche passage. Such an outline is of high interest for the estimation of possible hazards, mitigation and mapping. Fig. 6 outlines the maximum pressures of the Val Prada avalanche computed with the VS_{const}, VS_{SG} and the $VS_{extended}$ approaches (see Section 5.2) in RAMMS. A medium avalanche of about 75,000 m^3 release volume is used. The avalanche track has an approximate fall height of about 1300 m and an approximate length of 2500 m. The difference of the pressure based run outs for the three model approaches is clearly visible and can be on the order of 100 m or more. This shows that the overall friction parameter used in the VS_{SG} is substantially higher. The overall friction in the extended VS model is substantially lower than the VS_{SG}. This shows that VS_{SG} model utilized larger but physically less justified friction parameters. Furthermore, the pressure outlines for three different model approaches show that $VS_{constant} > VS_{extended} > VS_{SG}$. The extra terms in the frictional forces due to curvature lead to lower velocities and thus shorter run out distances using the extended model. This means that the overall extended $VS_{extended}$ model friction parameters induce higher friction than $VS_{constant}$ and lower friction than VS_{SG}. These observations are also explained in Fig. 5 more quantitatively.

As observed in Fig. 6, the variation in the extent of the pressure iso lines is in correspondence with the comparison of the friction values in the previous section. The VS_{const} (lowest friction values) appears to have the furthest extent of pressure iso lines, the VS_{SG} (highest overall friction) has contracting pressure iso lines, whereas the extended $VS_{extended}$ model is in between (both for the friction values and pressure outlines).

5.4. Discussion and implications of the new model

Although all the calibration work has already been done for avalanche simulations in the Swiss Alps, the extended Voellmy–Salm model (Eq. (4) with Eq. (18)) can still be important to improve the avalanche simulations by incorporating its additional effects (mainly via R_t) in the new simulations. Furthermore, it becomes even more important while calibrating the numerical software and avalanche simulation for other mountain regions in the world. Due to differences in general weather, snow and topographic conditions, a region specific calibration is possible.

6. Summary and conclusion

The classical Voellmy–Salm avalanche model and the computational tool RAMMS are based on the two empirical friction parameters

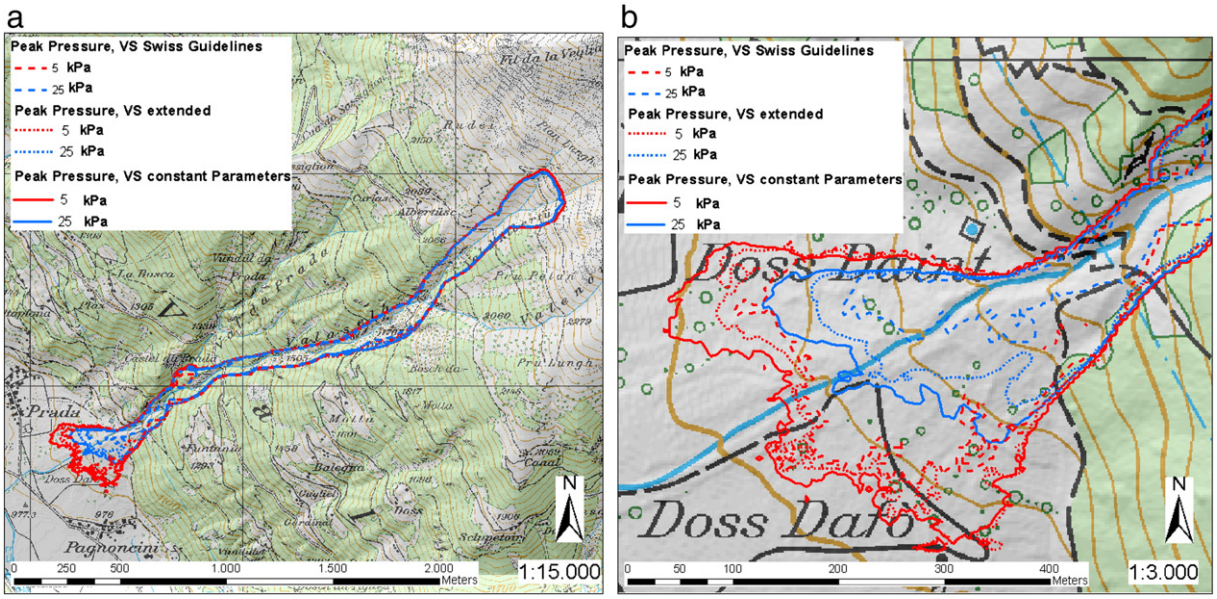

Fig. 6. Map and (DTM-AV ©2008 swisstopo (DV033492), map PK25 ©2008 swisstopo (DV033492)) results of a RAMMS simulation on the Val Prada avalanche track. Shown are the peak pressure iso lines for 5 kPa and 25 kPa, for a simulation with the $VS_{constant}$ (solid line), the $VS_{extended}$ (dotted line) and the VS_{SG} (dashed line) approaches respectively. (a) Shows the complete outline of the avalanche, (b) a detailed figure of the run out zone. There are substantial differences between the pressure iso lines produced by the different model approaches; the result of the $VS_{extended}$ lies between the results of $VS_{constant}$ and VS_{SG}.

μ and ξ representing the dry Coulomb friction and velocity dependent viscous drag (friction), respectively. The values of μ and ξ are determined through a calibration process that is partly based on a DEM analysis to distinguish between different terrain features such as open slope, channel or gully regions. Although the modeling results with RAMMS have been promising, μ and ξ still lack a physical explanation as they are empirical values. The real origin of the contribution of ξ to the basal topography and thus to the overall friction law is still open for discussion.

For a curved surface, the overburden pressure gains an extra term associated with the 'centrifugal force' induced by the curvature of the underlying topography. This leads to the enhancement of the basal friction by an extra term associated with the curvature that is attached to the square of the flow velocity (in additional to the classical Voellmy drag). The curvature contribution can be directly calculated from the DEM and a calibration step is not necessary. In contrast to the classical Voellmy–Salm friction relation in which the two friction parameters (μ and ξ) are empirical values that are accessible only through calibration, we decomposed the velocity dependent friction contribution into two parts and construct a curvature dependent friction law, here called the 'extended Voellmy–Salm model'. In this model there are three terms: the Coulomb friction, the new curvature correction and the classical Voellmy drag. This model, which mathematically and physically include the curvature effects into the Voellmy–Salm model, is then implemented in the RAMMS computational tool.

Three site-specific Swiss natural avalanche flow paths (Salezertobel, Vallee de la Sionne and Val Prada) are considered to compare the apparent (velocity dependent) frictional resistance of the extended Voellmy–Salm model to the classical Voellmy–Salm model. Our numerical simulation results demonstrate substantial effects of the curvature in the avalanche dynamics. The correlation between the extended Voellmy–Salm model and the classical Voellmy–Salm model (using the Swiss Guideline Calibration) highly depends on the flow path the avalanche assumes. The overall friction in the extended Voellmy–Salm model (with respect to the representative values of $\bar{\mu}$ and $\bar{\xi}$) is substantially lower than the Voellmy–Salm model (with calibrated values of μ and ξ according to the Swiss Guidelines). μ and ξ implicitly include the topographic curvature, but $\bar{\mu}$ and $\bar{\xi}$ are independent of curvature, because in the extended Voellmy–Salm model curvature is explicitly, separately and analytically included in the basal friction. This is the reason why the overall friction in the extended Voellmy–Salm model is lower than the classical Voellmy–Salm model, leading to a significant increase in the values and extension in the spatial distribution of pressure along the flow path in the new model. This shows that Voellmy–Salm model utilized larger friction parameters to additionally include the curvature effects. This highlights the importance of curvature effects in applied avalanche modeling as their values are now explicitly known and implemented. A complete implementation, however, requires new calibrations of the topography independent frictional coefficients $\bar{\mu}$ and $\bar{\xi}$, or some analytical description of these parameters are necessary.

Acknowledgment

This research work was carried out under the financial support of the German Academic Exchange Service (DAAD), SLF Davos, and the Department of Geodynamics and Geophysics, University of Bonn. We thank the referee for constructive comments that helped to substantially improve the clarity and quality of this paper.

References

Barbolini, M., Gruber, U., Keylock, C.J., Naaim, M., Savi, F., 2000. Application of statistical and hydraulic-continuum dense-snow avalanche models to five real european sites. Cold Regions Science and Technology 31 (2), 133–149.

Bartelt, P., Buser, O., 2010. Frictional relaxation in avalanches. Annals of Glaciology 51 (54), 98–104.

Bartelt, P., Buser, O., Platzer, K., 2006. Fluctuationdissipation relations for granular snow avalanches. Journal of Glaciology 52 (179), 631–643.

Bartelt, P., Buser, O., Platzer, K., 2007. Starving avalanches: frictional mechanisms at the tails of finite-sized mass movements. Geophysical Research Letters 34 (20), L20407.

Bartelt, P., Salm, B., Gruber, U., 1999. Calculating dense-snow avalanche runout using a voellmy-fluid model with active/passive longitudinal straining. Journal of Glaciology 45 (150), 242–254.

Bouchut, F., Mangeney-Castelnau, A., Perthame, B., Vilotte, J., 2003. A new model of Saint Venant and Savage-Hutter type for gravity driven shallow water flows. Comptes Rendus Mathematique 336 (6), 531–536.

Bouchut, F., Westdickenberg, M., 2004. Gravity driven shallow water models for arbitrary topography. Communications in Mathematical Sciences 2 (3), 359–389.

Buser, O., Bartelt, P., 2009. Production and decay of random kinetic energy in granular snow avalanches. Journal of Glaciology 55 (189), 3–12.

Christen, M., Kowalski, J., Bartelt, P., 2010. Ramms: numerical simulation of dense snow avalanches in three-dimensional terrain. Cold Regions Science and Technology 63, 1–14.

Cui, X., Gray, J.M.N.T., Jóhannesson, T., 2007. Deflecting dams and the formation of oblique shocks in snow avalanches at Flateyri, Iceland. Journal of Geophysical Research 112, F04012.

Denlinger, R.P., Iverson, R.M., 2004. Granular avalanches across irregular three-dimensional terrain: 1. theory and computation. Journal of Geophysical Research 109 (F1), F01014.

Gray, J.M.N.T., Cui, X., 2007. Weak, strong and detached oblique shocks in gravity-driven granular free-surface flows. Journal of Fluid Mechanics 579, 113–136.

Gray, J.M.N.T., Tai, Y.C., Noelle, S., 2003. Shock waves, dead zones and particle-free regions in rapid granular free-surface flows. Journal of Fluid Mechanics 491 (1), 161–181.

Gray, J.M.N.T., Wieland, M., Hutter, K., 1999. Gravity-driven free surface flow of granular avalanches over complex basal topography. Proceedings of the Royal Society of London. Series A: Mathematical, Physical and Engineering Sciences 455, 1841 (1985).

Gruber, U., Bartelt, P., 2007. Snow avalanche hazard modelling of large areas using shallow water numerical methods and gis. Environmental Modelling & Software 22 (10), 1472–1481.

Gruber, U., Margreth, S., 2001. Winter 1999: a valuable test of the avalanche-hazard mapping procedure in switzerland. Annals of Glaciology 32 (1), 328–332.

Hákonardóttir, K.M., Hogg, A.J., 2005. Oblique shocks in rapid granular flows. Physics of Fluids 17, 077101.

Hutter, K., Wang, Y., Pudasaini, S.P., 2005. The Savage-Hutter avalanche model: how far can it be pushed? *Philosophical Transactions of the Royal Society A: Mathematical*. Physical and Engineering Sciences 363 (1832), 1507.

Iverson, R.M., Logan, M., Denlinger, R.P., 2004. Granular avalanches across irregular three-dimensional terrain: 2. experimental tests. Journal of Geophysical Research 109 (F1), F01015.

Johnson, C.G., Gray, J.M.N.T., 2011. Granular jets and hydraulic jumps on an inclined plane. Journal of Fluid Mechanics 675 (1), 87–116.

Mangeney, A., Bouchut, F., Thomas, N., Vilotte, J., Bristeau, M., 2007. Numerical modeling of self-channeling granular flows and of their levee-channel deposits. Journal of Geophysical Research 112, 2017.

McDougall, S., Hungr, O., 2004. A model for the analysis of rapid landslide motion across three-dimensional terrain. Canadian Geotechnical Journal 41 (6), 1084–1097.

Patra, A., Bauer, A., Nichita, C., Pitman, E., Sheridan, M., Bursik, M., Rupp, B., Webber, A., Stinton, A., Namikawa, L., et al., 2005. Parallel adaptive numerical simulation of dry avalanches over natural terrain. Journal of Volcanology and Geothermal Research 139 (1–2), 1–21.

Pitman, E., Nichita, C., Patra, A., Bauer, A., Bursik, M., Weber, A., 2003a. A model of granular flows over an erodible surface. Discrete and Continuous Dynamical Systems Series B 3 (4), 589–600.

Pitman, E., Nichita, C., Patra, A., Bauer, A., Sheridan, M., Bursik, M., 2003b. Computing granular avalanches and landslides. Physics of fluids 15, 3638.

Platzer, K., Bartelt, P., Jaedicke, C., 2007. Basal shear and normal stresses of dry and wet snow avalanches after a slope deviation. Cold Regions Science and Technology 49 (1), 11–25.

Pouliquen, O., 1999a. On the shape of granular fronts down rough inclined planes. Physics of fluids 11, 1956.

Pouliquen, O., 1999b. Scaling laws in granular flows down rough inclined planes. Physics of fluids 11, 542–548.

Pouliquen, O., Forterre, Y., 2002. Friction law for dense granular flows: application to the motion of a mass down a rough inclined plane. Journal of Fluid Mechanics 453, 133–151.

Pudasaini, S.P., 2011. Some exact solutions for debris and avalanche flows. Physics of Fluids 23, 043301.

Pudasaini, S.P., Eckart, W., Hutter, K., 2003. Gravity-driven rapid shear flows of dry granular masses in helically curved and twisted channels. Mathematical Models and Methods in Applied Sciences 13 (7), 1019–1052.

Pudasaini, S.P., Hutter, K., 2003. Rapid shear flows of dry granular masses down curved and twisted channels. Journal of Fluid Mechanics 495 (−1), 193–208.

Pudasaini, S.P., Hutter, K., 2007. Avalanche dynamics: dynamics of rapid flows of dense granular avalanches. Springer, Berlin, New York.

Pudasaini, S.P., Kroener, C., 2008. Shock waves in rapid flows of dense granular materials: theoretical predictions and experimental results. Physical Review E 78 (4), 041308.

Pudasaini, S.P., Wang, Y., Hutter, K., 2005a. Modelling debris flows down general channels. Natural Hazards and Earth System Sciences 5, 799–819.

Pudasaini, S.P., Wang, Y., Hutter, K., 2005b. Rapid motions of free-surface avalanches down curved and twisted channels and their numerical simulation. Philosophical Transactions of the Royal Society A: Mathematical, Physical and Engineering Sciences 363 (1832), 1551.

Pudasaini, S.P., Wang, Y., Sheng, L., Hsiau, S., Hutter, K., Katzenbach, R., 2008. Avalanching granular flows down curved and twisted channels: theoretical and experimental results. Physics of Fluids 20, 073302.

Sailer, R., Fellin, W., Fromm, R., Jörg, P., Rammer, L., Sampl, P., Schaffhauser, A., 2008. Snow avalanche mass-balance calculation and simulation-model verification. Annals of Glaciology 48 (1), 183–192.

Salm, B. (1993). Flow, flow transition and runout distances of flowing avalanches. Annals Of Glaciology, Vol 18, 1993 — Proceedings Of The Symposium On Snow And Snow-Related Problems, 18:221–226.

Salm, B., Burkhard, A., Gubler, H.U., 1990. Berechnung von Fliesslawinen: Eine Anleitung fuer Praktiker; mit Beispielen. Mitteilungen des Eidgenoessischen Instituts fuer Schnee- und Lawinenforschung 47, 1–37.

Sampl, P., Zwinger, T., 2004. Avalanche simulation with samos. Annals of Glaciology 38 (1), 393–398.

Savage, S.B., Hutter, K., 1989. The motion of a finite mass of granular material down a rough incline. Journal of Fluid Mechanics 199 (1), 177–215.

Savage, S.B., Hutter, K., 1991. The dynamics of avalanches of granular materials from initiation to runout. Part I: analysis. Acta Mechanica 86 (1), 201–223.

Sovilla, B., Schaer, M., Rammer, L., 2008. Measurements and analysis of full-scale avalanche impact pressure at the Vallee de la Sionne test site. Cold Regions Science and Technology 51 (2–3), 122–137.

Voellmy, A., 1955. Über die Zerstörungskraft von Lawinen. Schweizerische Bauzeitung, Sonderdruck aus dem 73, 1–25 Jahrgang(12, 15, 17, 19 und 37).

Wieland, M., Gray, J.M.N.T., Hutter, K., 1999. Channelized free-surface flow of cohesionless granular avalanches in a chute with shallow lateral curvature. Journal of Fluid Mechanics 392, 73–100.